

Supporting Information (SI)

Simulation of SOA Formation from the Photooxidation of Monoalkylbenzenes in the Presence of Aqueous Aerosols Containing Electrolytes under Various NO_x Levels

Chufan Zhou, Myoseon Jang, and Zechen Yu

Department of Environmental Engineering Sciences, University of Florida, P.O. Box 116450,
Gainesville, FL 32611, USA

Correspondence to: Myoseon Jang (mjang@ufl.edu)

Number of tables: 3

Number of figures: 8

Section S2. Estimation of the atomic oxygen-to-carbon ratio ($O:C_i$) and molecular weight (MW_i) for each lumping species

Due to the increase in complexity from parameterizing $O:C_i$ and MW_i as a function of HC/NO_x , we assume that the $O:C_i$ and MW_i are linearly related to the NO_x level, which is ranging from $HC/NO_x=2$ (high NO_x level (H- NO_x)) to $HC/NO_x=14$ (the low NO_x level (L- NO_x)). The calculation of the $O:C_i$ is exemplified in the following part in this Section.

Based on the simulations from the near-explicit gas kinetic model under the same metrological condition (6/19/2015), four sets of $O:C_i$ are carried out under four conditions: $O:C_{i\ fresh\ H-NO_x}$ ($f_A=-7.6$), $O:C_{i\ highly\ aged\ H-NO_x}$ ($f_A=-5.2$), $O:C_{i\ fresh\ L-NO_x}$ ($f_A=-3.7$), and $O:C_{i\ highly\ aged\ L-NO_x}$ ($f_A=-2.9$), where the f_A is the aging factor, which is defined as shown in Eq. 1 in the manuscript. Thus, the fresh set of $O:C_i$ ($O:C_{i\ fresh}$) under given NO_x conditions can be approached by the similar weighted average method (Section 3.2.2 in the manuscript) by combining the two sets of $O:C_{i\ fresh\ H-NO_x}$ and $O:C_{i\ fresh\ L-NO_x}$, as is shown in Eq. S2. The fractional weighting factor (f_{NO_x}' : 0-1) is estimated by scaling the given HC/NO_x within the upper boundary ($HC/NO_x=14$) and the lower ($HC/NO_x=2$) boundary. Similarly, the highly aged set of $O:C_i$ ($O:C_{i\ highly\ aged}$) can be obtained by combining $O:C_{i\ highly\ aged\ H-NO_x}$ and $O:C_{i\ highly\ aged\ L-NO_x}$ using f_{NO_x}' , as shown in Eq. S3.

$$O:C_{i\ fresh} = (1 - f_{NO_x}') \cdot O:C_{i\ fresh\ H-NO_x} + f_{NO_x}' \cdot O:C_{i\ fresh\ L-NO_x} \quad (S2)$$

$$O:C_{i\ highly\ aged} = (1 - f_{NO_x}') \cdot O:C_{i\ highly\ aged\ H-NO_x} + f_{NO_x}' \cdot O:C_{i\ highly\ aged\ L-NO_x} \quad (S3)$$

Since the change of the $O:C_i$ of the lumping species, i , is due to the evolution of the gas-phase products, which is governed by the α_i , the dynamic $O:C_i$ set can be simply estimated by comprising the $O:C_{i\ fresh}$ and $O:C_{i\ highly\ aged}$ using the fractional aging factor, f_A' , as shown in Eq. S4 (same method in Eq. 2 in the manuscript).

$$\text{dynamic } O:C_i = (1 - f_A') \cdot O:C_{i\ fresh} + (f_A') \cdot O:C_{i\ highly\ aged} \quad (S4)$$

The calculation of the dynamic MW_i set follows the exact same method used for the dynamic $O:C_i$ set. The dynamic $O:C_i$ set and dynamic MW_i set are directly applied to estimate the activity coefficient of the organics in the inorganic (*in*) phase, as shown in Eq. 4 in the manuscript.

Section S3. Calculation of the activity coefficient in aqueous solutions containing electrolytes

As is described in Section 3.2 in the manuscript, 16 organic compounds (O:C ranging from 0.13 to 0.8) with various functional groups and molecular size (MW) were chosen to estimate the activity coefficient ($\gamma_{in,i}$) of the organics in the inorganic phase. The inorganic phase compositions (FS) and ambient humidity (RH) are ranged from 0.33 to 1 and 0.1 to 0.8, respectively, to cover our experimental conditions. The Aerosol Inorganic-Organic Mixtures Functional Groups Activity Coefficients (AIOMFAC) (Zuend et al., 2011) was run for the highest concentration of the 16 selected organic compounds, where $\gamma_{in,i}$ was as close to unity as possible in the inorganic $\text{SO}_4^{2-}\text{-NH}_4^+\text{-H}_2\text{O}$ system. Thus, the resulting $\gamma_{in,i}$ was fit to the $\ln(\text{RH})$, FS, O:C, and MW to generate the regression equation (Eq. 4 in the manuscript) for the relatively nonpolar compound (O:C < 0.8), as shown in Fig. S7. The resulting R^2 is 0.5742. For the $\gamma_{in,i}$ of the relatively polar compounds (O:C > 0.8), Eq. S5, which was generated by Beardsley and Jang (2016) for isoprene products, was applied.

$$\gamma_{in,i} = e^{0.050 \cdot \ln(100 \cdot \text{RH}) - 0.011 \cdot \text{org:sul} - 0.252 \cdot \text{O:C}_i + 0.007 \cdot \text{MW}_i - 0.229}, \quad (\text{S5})$$

where org:sul represents the bulk organic-to-sulfate mass ratio.

Section S4. Measurement of aerosol acidity using the C-RUV technique

In the presence of organic matter (OM), the acidity (proton concentration: $[H^+]$, mol L⁻¹ of aerosol) reduction in acidic aerosols could be considered by two forces: (1) the neutralization with atmospheric ammonia and (2) the formation of alkyl substituted sulfates, which includes monoalkyl sulfates and dialkyl sulfates (diOS). Due to the strong acidity of monoalkyl sulfates, we only attributed the reductions in aerosol acidity and hygroscopicity to the formation of diOS. Using the inorganic concentrations measured by the PILS-IC, where organosulfate was reversed to sulfate ion due to high-temperatures (> 80 °C) water vapor, the proton concentration, which results only from ammonia neutralization, can be predicted through the inorganic thermodynamic model EAIM-II (Clegg and Seinfeld, 2006). The proton concentration, which was associated with both ammonia neutralization and diOS formation, was measured by colorimetry integrated with the reflectance UV-visible spectrometer (C-RUV) technique (Jang et al., 2008; Li et al., 2016; Li and Jang, 2012), which utilized a UV-visible spectrometer in absorbance mode to detect the color change on a sample-collected dyed filter. Thus, the difference between the two measured $[H^+]$ values is due to the formation of diOS. The reduction in sulfate concentration, which equalizes the PILS-IC measured $[H^+]$ to the C-RUV measured $[H^+]$, is the measured diOS concentration ($[diOS]_{exp}$). The C-RUV method has been previously applied to toluene and 1,3,5-trimethylbenzene SOAs (Im et al. (2014) and isoprene SOA (Beardsley and Jang (2016)).

Section S5. Derivation of the model equations used to predict the organic mass

The gas-organic phase partitioning coefficient ($K_{or,i}$, $\text{m}^3 \mu\text{g}^{-1}$) and the gas-inorganic phase partitioning coefficient ($K_{in,i}$, $\text{m}^3 \mu\text{g}^{-1}$) of each species are obtained from Eq. 3 in the manuscript. The concentrations ($C_{g,i}$, $C_{or,i}$, and $C_{in,i}$: $\mu\text{g m}^{-3}$ of air) of each lumping species in the gas (g), organic aerosol (or), and inorganic (in) phases can be derived from the Eqs. S6, S7, and S8, respectively. The partitioning and aerosol-phase reactions in the multiphase system (g , or , and in phase) can be kinetically represented as shown in Fig. S8.

$$C_{g,i} = \frac{C_{T,i}}{1 + K_{or,i} OM_T + K_{in,i} M_{in}}, \quad (\text{S6})$$

$$C_{or,i} = \frac{C_{T,i} K_{or,i} OM_T}{1 + K_{or,i} OM_T + K_{in,i} M_{in}}, \quad (\text{S7})$$

$$C_{in,i} = \frac{C_{T,i} K_{in,i} M_{in}}{1 + K_{or,i} OM_T + K_{in,i} M_{in}}, \quad (\text{S8})$$

where the subscript i represents the lumping species, i . $C_{T,i}$ is the total organics concentration in multiple phases (i.e., $C_{T,i} = C_{g,i} + C_{or,i} + C_{in,i}$). OM_T and M_{in} are the mass concentration ($\mu\text{g m}^{-3}$ of air) of the total organic matter and the total inorganic aerosol, respectively.

The formation of organic matter (ΔOM_{AR}) through aerosol-phase reactions are described by two processes: (1) the oligomerization in or phase and (2) the oligomerization in in phase (i.e., acid-catalyzed reaction). The two reactions are described based on the second-order kinetic self-dimerization as shown in Eqs. S9 and S10.

$$\frac{dC_{or,i}}{dt} = -k_{o,i} C'_{or,i}{}^2 \left(\frac{MW_i OM_T}{\rho_{or} 10^3} \right), \quad (\text{S9})$$

$$\frac{dC_{in,i}}{dt} = -k_{AC,i} C'_{in,i}{}^2 \left(\frac{MW_i M_{in}}{\rho_{in} 10^3} \right), \quad (\text{S10})$$

where $C'_{or,i}$ and $C'_{in,i}$ are the aerosol-base organic concentration (mol L^{-1}) in in phase and or phase, respectively. $k_{o,i}$ and $k_{AC,i}$ are the second order reaction rate constant ($\text{L mol}^{-1} \text{s}^{-1}$) for oligomerization in the or phase and the in phase, respectively. The conversion of the aerosol-base concentration ($C'_{or,i}$ and $C'_{in,i}$) (mol L^{-1}) to air-base concentration ($C_{or,i}$ and $C_{in,i}$) ($\mu\text{g m}^{-3}$) is fulfilled by the bracketed terms, $\frac{MW_i OM_T}{\rho_{or} 10^3}$ and $\frac{MW_i M_{in}}{\rho_{in} 10^3}$, respectively. MW_i is the molecular weight of species, i . OM_T is the total organic matter (OM) concentration ($\mu\text{g m}^{-3}$). ρ_{or} and ρ_{in} are the densities (g cm^{-3}) of the or phase aerosol and in phase aerosol.

Based on the mass balance, ΔOM_{AR} is same as the consumed total concentrations of lumping species (sum up of $C_{T,i}$ of each lumping species, i) as shown in the following equation.

$$\Delta OM_{AR} = -\sum_i \Delta C_{T,i} = -\sum_i \int dC_{T,i}, \quad (S11)$$

Thus, the following equations can be applied to kinetically express partitioning and in-particle chemistry processes of the lumping species.

$$\frac{dC_{g,i}}{dt} = k_{11}C_{or,i} - k_{12}C_{g,i} + k_{21}C_{in,i} - k_{22}C_{g,i}, \quad (S12)$$

$$\frac{dC_{or,i}}{dt} = -k_{11}C_{or,i} + k_{12}C_{g,i} - k_{31}C_{or,i} + k_{32}C_{in,i} - k_{o,i}C'_{or,i}{}^2 \left(\frac{MW_i OM_T}{\rho_{or} 10^3}\right), \quad (S13)$$

$$\frac{dC_{in,i}}{dt} = -k_{21}C_{in,i} + k_{22}C_{g,i} + k_{31}C_{or,i} - k_{32}C_{in,i} - k_{AC,i}C'_{in,i}{}^2 \left(\frac{MW_i M_{in}}{\rho_{in} 10^3}\right), \quad (S14)$$

where k_{nm} is the first-order reaction rate constants (S^{-1}) ($n = 1, 2, 3; m = 1, 2$) in which each couple of them denotes the equilibrium among $C_{g,i}$, $C_{or,i}$ and $C_{in,i}$ as shown in Fig. S8.

From Eqs. S12–S14, $\frac{dC_{T,i}}{dt}$ can be rewritten as following,

$$\frac{dC_{T,i}}{dt} = \frac{dC_{g,i}}{dt} + \frac{dC_{or,i}}{dt} + \frac{dC_{in,i}}{dt} = -k_{o,i}C'_{or,i}{}^2 \left(\frac{MW_i OM_T}{\rho_{or} 10^3}\right) - k_{AC,i}C'_{in,i}{}^2 \left(\frac{MW_i M_{in}}{\rho_{in} 10^3}\right), \quad (S15)$$

Eq. S15 can be rearranged with respect to $C_{T,i}$ by plugging Eqs. S7 and S8 as following.

$$\frac{dC_{T,i}}{dt} = \left(k_{o,i} \frac{\rho_{or} 10^3 OM_T K_{or,i}^2}{MW_i (1 + K_{or,i} OM_T + K_{in,i} M_{in})^2} + k_{AC,i} \frac{\rho_{in} 10^3 M_{in} K_{in,i}^2}{MW_i (1 + K_{or,i} OM_T + K_{in,i} M_{in})^2} \right) C_{T,i}^2, \quad (S16)$$

Based on the assumption that OM_T , M_{in} , $k_{o,i}$, and $k_{AC,i}$ are constants during each computational time step, Eq. S16 can be solved as following by being integrated as a second-order differential equation.

$$\Delta OM_{AR} = -\sum_i \Delta C_{T,i} = -\sum_i \int_0^{\Delta t} (k_{o,i}\beta_{1,i} + k_{AC,i}\beta_{2,i})C_{T,i}^2, \quad (S17)$$

where $\beta_{1,i} = \frac{\rho_{or} 10^3 OM_T K_{or,i}^2}{MW_i (1 + K_{or,i} OM_T + K_{in,i} M_{in})^2}$ and $\beta_{2,i} = \frac{\rho_{in} 10^3 M_{in} K_{in,i}^2}{MW_i (1 + K_{or,i} OM_T + K_{in,i} M_{in})^2}$ are the simplified terms associating with oligomerization in the *or* phase and the *in* phase, respectively. Hence, the analytical solution corresponding to ΔOM_{AR} can be achieved as shown in the following equation.

$$\Delta OM_{AR} = -\sum_i \Delta C_{T,i} = -\sum_i \frac{C_{T,i}^2 \Delta t (k_{o,i}\beta_{1,i} + k_{AC,i}\beta_{2,i})}{C_{T,i} \Delta t (k_{o,i}\beta_{1,i} + k_{AC,i}\beta_{2,i}) + 1}, \quad (S18)$$

Reference

Beardsley, R. L., and Jang, M.: Simulating the SOA formation of isoprene from partitioning and aerosol phase reactions in the presence of inorganics, *Atmospheric Chemistry and Physics*, 16, 5993-6009, 10.5194/acp-16-5993-2016, 2016.

Clegg, S. L., and Seinfeld, J. H.: Thermodynamic models of aqueous solutions containing inorganic electrolytes and dicarboxylic acids at 298.15 K. 2. Systems including dissociation equilibria, *J Phys Chem A*, 110, 5718-5734, 10.1021/jp056150j, 2006.

Im, Y., Jang, M., and Beardsley, R. L.: Simulation of aromatic SOA formation using the lumping model integrated with explicit gas-phase kinetic mechanisms and aerosol-phase reactions, *Atmospheric Chemistry and Physics*, 14, 4013-4027, 10.5194/acp-14-4013-2014, 2014.

Jang, M., Czoschke, N. M., Lee, S., and Kamens, R. M.: Heterogeneous atmospheric aerosol production by acid-catalyzed particle-phase reactions, *Science*, 298, 814-817, 10.1126/science.1075798, 2002.

Jang, M., Cao, G., and Paul, J.: Colorimetric particle acidity analysis of secondary organic aerosol coating on submicron acidic aerosols, *Aerosol Science and Technology*, 42, 409-420, 10.1080/02786820802154861, 2008.

Jang, M. S., and Kamens, R. M.: Characterization of secondary aerosol from the photooxidation of toluene in the presence of NO_x and 1-propene, *Environmental Science & Technology*, 35, 3626-3639, 10.1021/es010676+, 2001.

Li, J., Jang, M., and Beardsley, R. L.: Dialkylsulfate formation in sulfuric acid-seeded secondary organic aerosol produced using an outdoor chamber under natural sunlight, *Environmental Chemistry*, 13, 590-601, 2016.

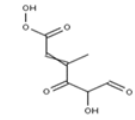
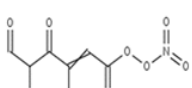
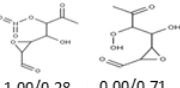
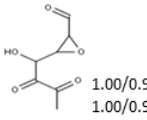
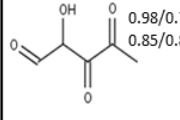
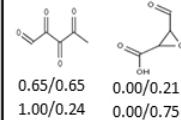
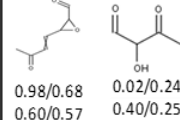
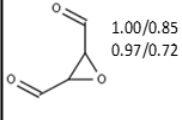
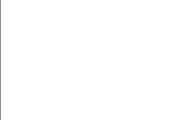
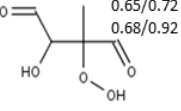
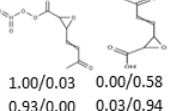
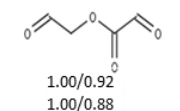
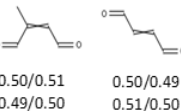
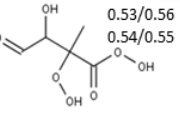
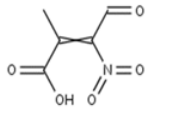
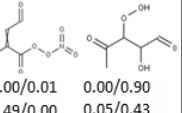
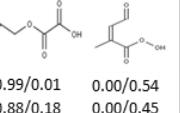
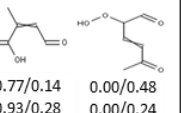
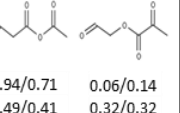
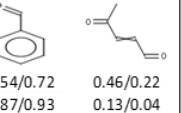
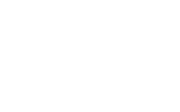
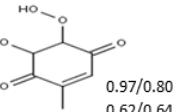
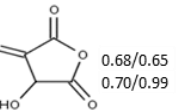
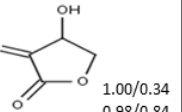
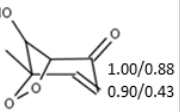
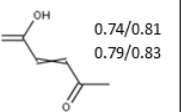
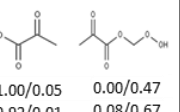
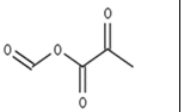
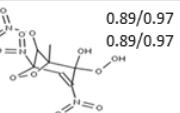
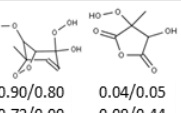
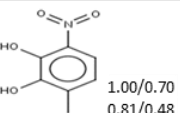
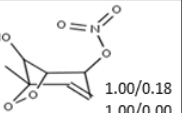
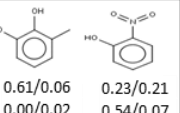
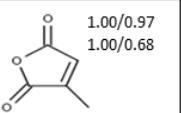
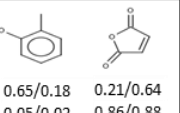
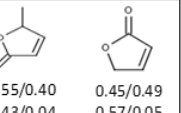
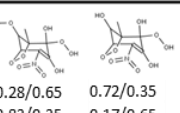
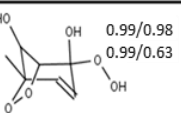
Li, J. Y., and Jang, M.: Aerosol Acidity Measurement Using Colorimetry Coupled With a Reflectance UV-Visible Spectrometer, *Aerosol Science and Technology*, 46, 833-842, 10.1080/02786826.2012.669873, 2012.

Stein, S. E., and Brown, R. L.: Estimation of Normal Boiling Points from Group Contributions, *J Chem Inf Comp Sci*, 34, 581-587, Doi 10.1021/Ci00019a016, 1994.

Zhao, L. W., Li, P., and Yalkowsky, S. H.: Predicting the entropy of boiling for organic compounds, *J Chem Inf Comp Sci*, 39, 1112-1116, Doi 10.1021/Ci990054w, 1999.

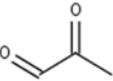
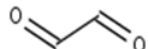
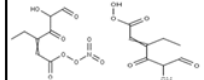
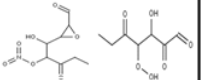
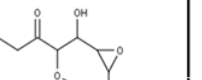
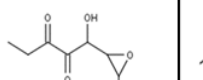
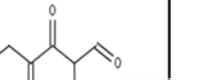
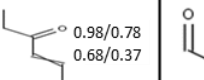
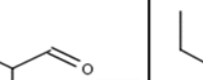
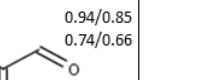
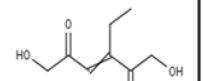
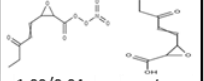
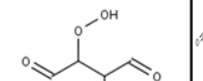
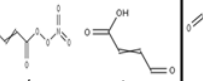
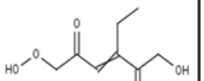
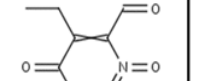
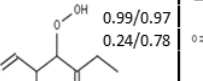
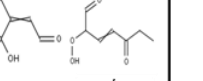
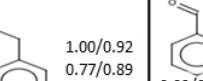
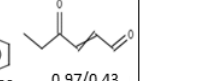
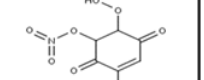
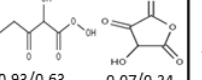
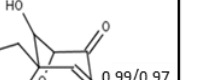
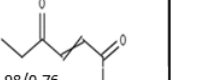
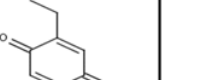
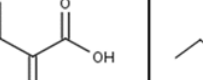
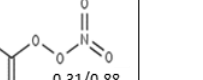
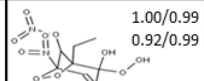
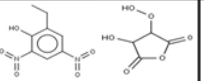
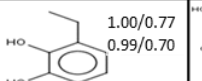
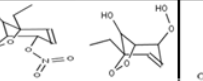
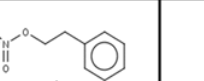
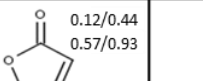
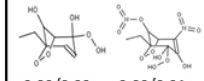
Zuend, A., Marcolli, C., Booth, A. M., Lienhard, D. M., Soonsin, V., Krieger, U. K., Topping, D. O., McFiggans, G., Peter, T., and Seinfeld, J. H.: New and extended parameterization of the thermodynamic model AIOMFAC: calculation of activity coefficients for organic-inorganic mixtures containing carboxyl, hydroxyl, carbonyl, ether, ester, alkenyl, alkyl, and aromatic functional groups, *Atmospheric Chemistry and Physics*, 11, 9155-9206, 10.5194/acp-11-9155-2011, 2011.

Table S1. Major oxygenated products distribution in gas phase for toluene oxidation under four conditions (i.e., high NO_x fresh, low NO_x fresh, high NO_x aged, and low NO_x aged). High NO_x: HC/NO_x=2; low NO_x: HC/NO_x=14.

$\alpha_{m,n}$		Toluene: Vapor Pressure (mmHg) [n]												
		n = 1 (10 ⁻⁸)	n = 2 (10 ⁻⁶)	n = 3 (10 ⁻⁵)	n = 4 (10 ⁻⁴)	n = 5 (10 ⁻³)	n = 6 (10 ⁻²)	n = 7 (10 ⁻¹)	n = 8 (10 ⁰)					
Reactivity [m]	R						IEPOX	MGLY	GLY					
	VF	 0.98/0.79 0.85/0.83	 1.00/0.28 1.00/0.02	 0.00/0.71 0.00/0.68	 1.00/0.99 1.00/0.96	 0.65/0.65 1.00/0.24	 0.00/0.21 0.00/0.75	 0.98/0.68 0.60/0.57	 0.02/0.24 0.40/0.25	 1.00/0.85 0.97/0.72				
	F				 0.65/0.72 0.68/0.92	 1.00/0.03 0.93/0.00	 0.00/0.58 0.03/0.94	 1.00/0.92 1.00/0.88	 0.50/0.51 0.49/0.50	 0.50/0.49 0.51/0.50				
	M	 0.53/0.56 0.54/0.55		 1.00/0.01 0.49/0.00	 0.00/0.90 0.05/0.43	 0.99/0.01 0.88/0.18	 0.00/0.54 0.00/0.45	 0.77/0.14 0.93/0.28	 0.00/0.48 0.00/0.24	 0.94/0.71 0.49/0.41	 0.06/0.14 0.32/0.32	 0.54/0.72 0.87/0.93	 0.46/0.22 0.13/0.04	
	S		 0.97/0.80 0.62/0.64	 0.68/0.65 0.70/0.99	 1.00/0.34 0.98/0.84	 1.00/0.88 0.90/0.43	 0.74/0.81 0.79/0.83	 1.00/0.05 0.92/0.01	 0.00/0.47 0.08/0.67	 1.00/0.97 1.00/0.68	 0.65/0.18 0.05/0.02	 0.21/0.64 0.86/0.88	 0.55/0.40 0.43/0.04	 0.45/0.49 0.57/0.05
	P	 0.89/0.97 0.89/0.97	 0.90/0.80 0.72/0.00	 0.04/0.05 0.09/0.44	 1.00/0.70 0.81/0.48	 1.00/0.18 1.00/0.00	 0.61/0.06 0.00/0.02	 0.23/0.21 0.54/0.07	 1.00/0.97 1.00/0.68	 0.65/0.18 0.05/0.02	 0.21/0.64 0.86/0.88	 0.55/0.40 0.43/0.04	 0.45/0.49 0.57/0.05	
	MA	 0.28/0.65 0.83/0.35	 0.72/0.35 0.17/0.65	 0.99/0.98 0.99/0.63										

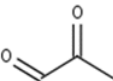
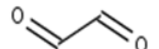
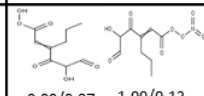
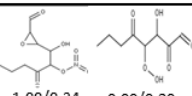
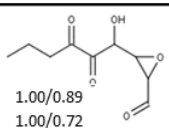
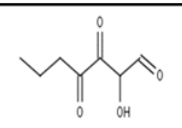
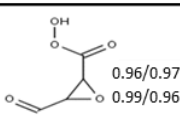
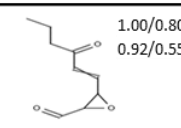
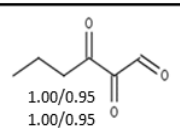
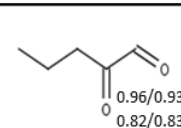
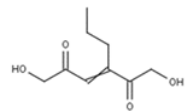
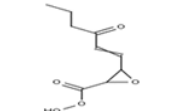
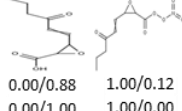
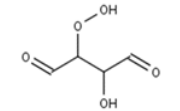
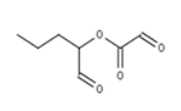
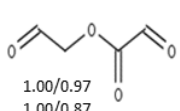
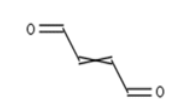
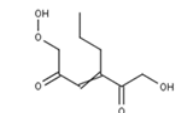
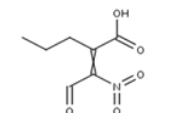
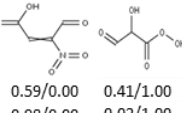
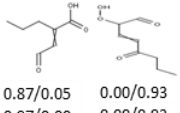
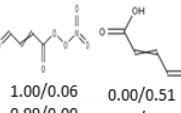
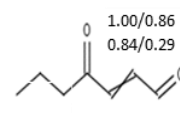
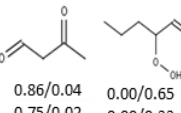
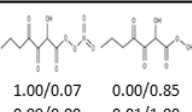
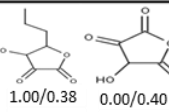
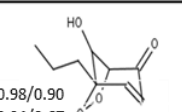
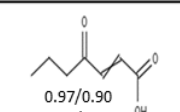
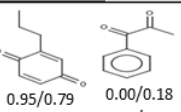
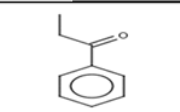
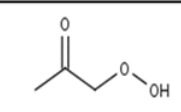
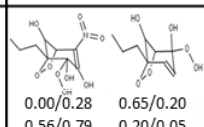
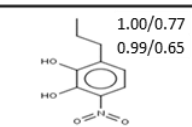
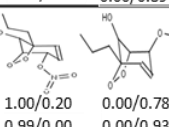
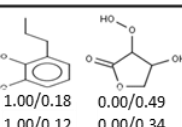
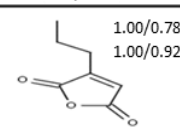
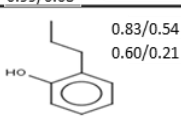
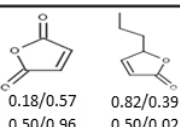
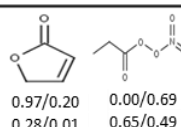
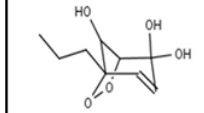
The number in the cells denotes the mass fraction of the product to the lumping species under conditions of high NO_x fresh, low NO_x fresh, high NO_x aged, and low NO_x aged, respectively (from left to right, top to bottom). No number indicates the organic compound is the major contributor (mass fraction > 0.9) regardless of the NO_x condition. Some of the trivial products were not listed.

Table S2. Major oxygenated products distribution in gas phase for ethylbenzene oxidation under four conditions (i.e., high NO_x fresh, low NO_x fresh, high NO_x aged, and low NO_x aged). High NO_x: HC/NO_x=2; low NO_x: HC/NO_x=14.

$\alpha_{m,n}$		Ethylbenzene: Vapor Pressure (mmHg) [n]								
		n = 1 (10 ⁻⁸)	n = 2 (10 ⁻⁶)	n = 3 (10 ⁻⁵)	n = 4 (10 ⁻⁴)	n = 5 (10 ⁻³)	n = 6 (10 ⁻²)	n = 7 (10 ⁻¹)	n = 8 (10 ⁰)	
Reactivity [m]	R						IEPOX	MGLY 	GLY 	
	VF	 1.00/0.07 0.98/0.00	 1.00/0.92 0.00/0.08 1.00/0.01 0.00/0.99	 1.00/0.95 0.89/0.76	 1.00/0.99 1.00/0.98	 0.99/0.56 0.94/0.63	 0.98/0.78 0.68/0.37	 0.97/0.21 0.53/0.88	 0.94/0.85 0.74/0.66	
	F				 1.00/0.04 0.97/0.00	 0.00/0.46 0.01/0.82	 0.99/0.97 0.24/0.78	 1.00/0.03 0.98/0.00	 0.00/0.53 0.01/0.91	 0.50/0.53 0.50/0.42 0.64/0.58 0.36/0.29
	M				 0.99/0.97 0.24/0.78	 0.91/0.14 0.90/0.00	 0.00/0.84 0.00/0.52	 1.00/0.92 0.77/0.89	 0.03/0.29 0.76/0.61	 0.97/0.43 0.24/0.03
	S		 0.93/0.63 0.37/0.01	 0.07/0.34 0.55/0.98	 0.99/0.97 0.60/0.72	 0.98/0.76 0.96/0.91				 0.31/0.88 0.92/0.61
	P	 1.00/0.99 0.92/0.99	 1.00/0.14 1.00/0.05	 1.00/0.77 0.99/0.70	 1.00/0.16 1.00/0.00	 0.00/0.71 0.00/0.61	 0.20/0.50 0.98/0.24	 1.00/0.24 0.62/0.02	 0.12/0.44 0.57/0.93	
	MA	 0.99/0.33 0.06/0.09	 0.00/0.31 0.69/0.07							

The number in the cells denotes the mass fraction of the product to the lumping species under conditions of high NO_x fresh, low NO_x fresh, high NO_x aged, and low NO_x aged, respectively (from left to right, top to bottom). No number indicates the organic compound is the major contributor (mass fraction > 0.9) regardless of the NO_x condition. Some of the trivial products were not listed.

Table S3. Major oxygenated products ocim in gas phase for n-propylbenzene under four conditions (i.e., high NO_x fresh, low NO_x fresh, high NO_x aged, and low NO_x aged). High NO_x: HC/NO_x=2; low NO_x: HC/NO_x=14.

$\alpha_{m,n}$		Propylbenzene: Vapor Pressure (mmHg) [n]							
		n = 1 (10 ⁻⁸)	n = 2 (10 ⁻⁶)		n = 3 (10 ⁻⁵)	n = 4 (10 ⁻⁴)	n = 5 (10 ⁻³)	n = 6 (10 ⁻²)	n = 7 (10 ⁻¹)
Reactivity [m]	R						IEPOX	MGLY 	GLY 
	VF	 0.00/0.87 1.00/0.13 0.00/1.00 1.00/0.00	 1.00/0.34 0.00/0.20 1.00/0.00 0.00/0.64	 1.00/0.89 1.00/0.72		 0.96/0.97 0.99/0.96	 1.00/0.80 0.92/0.55	 1.00/0.95 1.00/0.95	 0.96/0.93 0.82/0.83
	F			 0.00/0.88 1.00/0.12 0.00/1.00 1.00/0.00		 0.87/0.05 0.00/0.93 0.97/0.00 0.00/0.93	 1.00/0.06 0.00/0.51 0.99/0.00 0.00/0.92	 1.00/0.86 0.84/0.29	 0.86/0.04 0.00/0.65 0.75/0.02 0.00/0.33
	M			 0.59/0.00 0.41/1.00 0.98/0.00 0.02/1.00	 0.98/0.90 0.94/0.67	 0.97/0.90 0.99/0.71	 0.95/0.79 0.00/0.18 0.99/0.08 0.00/0.91		
	S		 1.00/0.07 0.00/0.85 0.99/0.00 0.01/1.00	 1.00/0.38 0.00/0.40 1.00/0.10 0.00/0.89		 1.00/0.78 1.00/0.92	 0.83/0.54 0.60/0.21	 0.18/0.57 0.82/0.39 0.50/0.96 0.50/0.02	 0.97/0.20 0.00/0.69 0.28/0.01 0.65/0.49
	P	 0.00/0.28 0.65/0.20 0.56/0.79 0.20/0.05	 1.00/0.77 0.99/0.65	 1.00/0.20 0.00/0.78 0.99/0.00 0.00/0.93	 1.00/0.18 0.00/0.49 1.00/0.12 0.00/0.34				
	MA								

The number in the cells denotes the mass fraction of the product to the lumping species under conditions of high NO_x fresh, low NO_x fresh, high NO_x aged, and low NO_x aged, respectively (from left to right, top to bottom). No number indicates the organic compound is the major contributor (mass fraction > 0.9) regardless of the NO_x condition. Some of the trivial products were not listed.

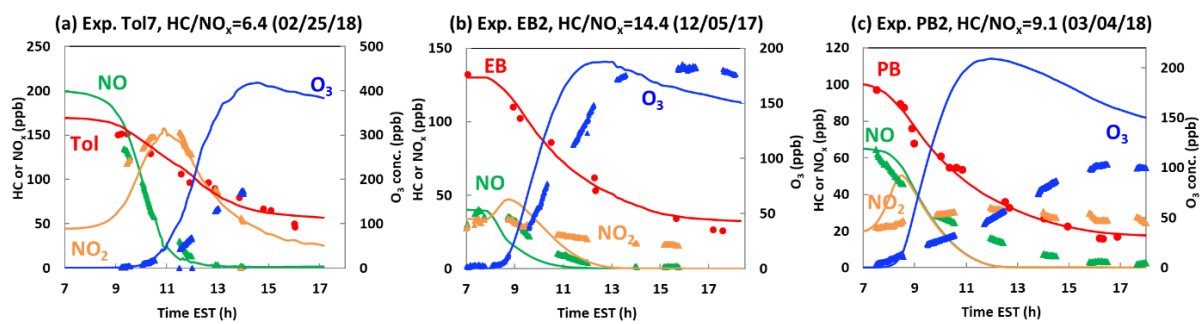


Figure S1: Time profiles of experimental measurements and simulation for three different hydrocarbons (HC): (a) toluene (Tol), (b) ethylbenzene (EB), and (c) n-propylbenzene (PB), along with O₃, NO₂, and NO concentration. The experimental conditions are available in Table 1.

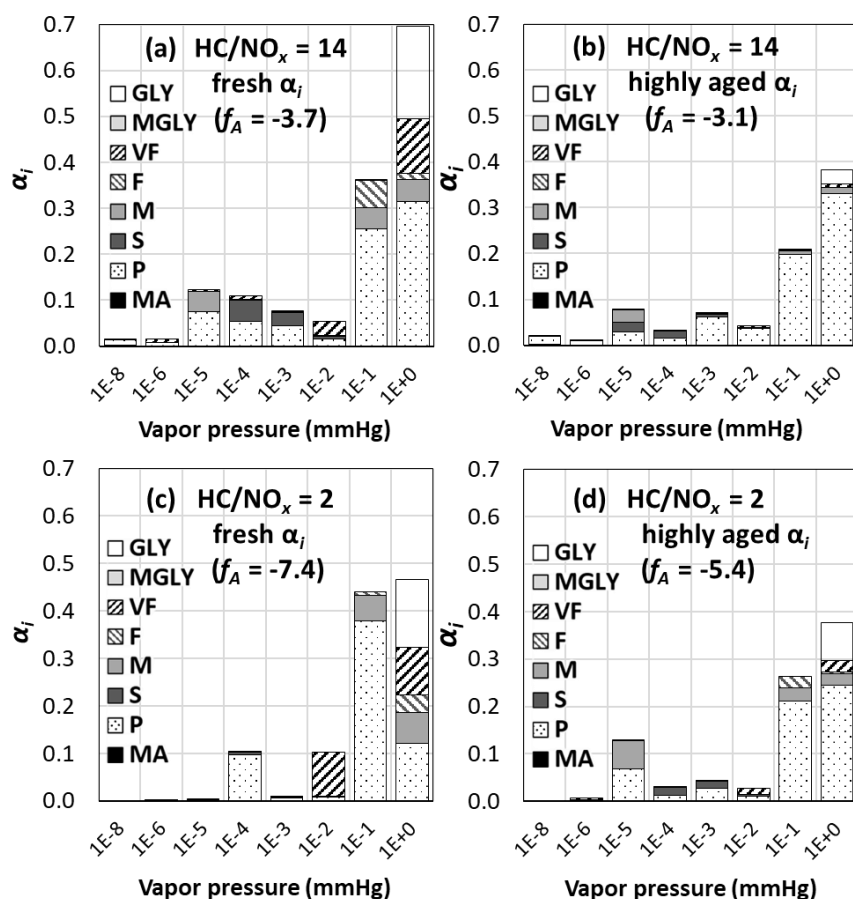


Figure S2: The mass-based stoichiometric coefficients (α_i) of each species, i , from ethylbenzene oxidation under low NO_x level (simulation based on the sunlight of Exp. Tol9, 06/14/18) at (a) fresh condition and (b) highly aged condition, and under high NO_x level at (c) fresh condition and (d) highly aged condition, where f_A is the aging factor as derived in Eq. 1. The oxygenated products predicted by the explicit gas kinetic model are lumped as a function of vapor pressure (8 groups: 10^{-8} , 10^{-6} , 10^{-5} , 10^{-4} , 10^{-3} , 10^{-2} , 10^{-1} , and 1 mmHg) and aerosol phase reactivity (6 groups), i.e., very fast (VF: tricarboxyls and α -hydroxybicycboxyls), fast (F: 2 epoxides or aldehydes), medium (M: 1 epoxide or aldehyde), slow (S: ketones), partitioning only (P), and multialcohol (MA). MGLY (methylglyoxal) and GLY (glyoxal) were lumped separately due to the relatively high reactivity.

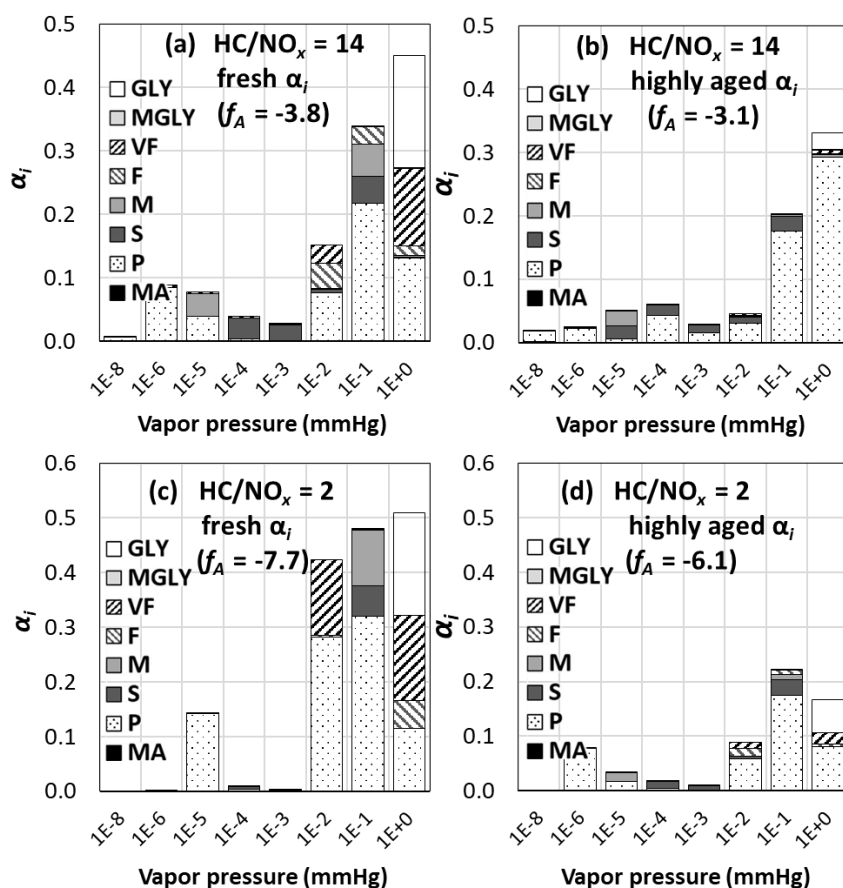


Figure S3: The mass-based stoichiometric coefficients (α_i) of each species, i , from n-propylbenzene oxidation under low NO_x level (simulation based on the sunlight of Exp. Tol9, 06/14/18) at (a) fresh condition and (b) highly aged condition, and under high NO_x level at (c) fresh condition and (d) highly aged condition, where f_A is the aging factor as derived in Eq. 1. The oxygenated products predicted by the explicit gas kinetic model are lumped as a function of vapor pressure (8 groups: 10^{-8} , 10^{-6} , 10^{-5} , 10^{-4} , 10^{-3} , 10^{-2} , 10^{-1} , and 1 mmHg) and aerosol phase reactivity (6 groups), i.e., very fast (VF: tricarbonyls and α -hydroxybicycbonyls), fast (F: 2 epoxides or aldehydes), medium (M: 1 epoxide or aldehyde), slow (S: ketones), partitioning only (P), and multialcohol (MA). MGLY (methylglyoxal) and GLY (glyoxal) were lumped separately due to the relatively high reactivity.

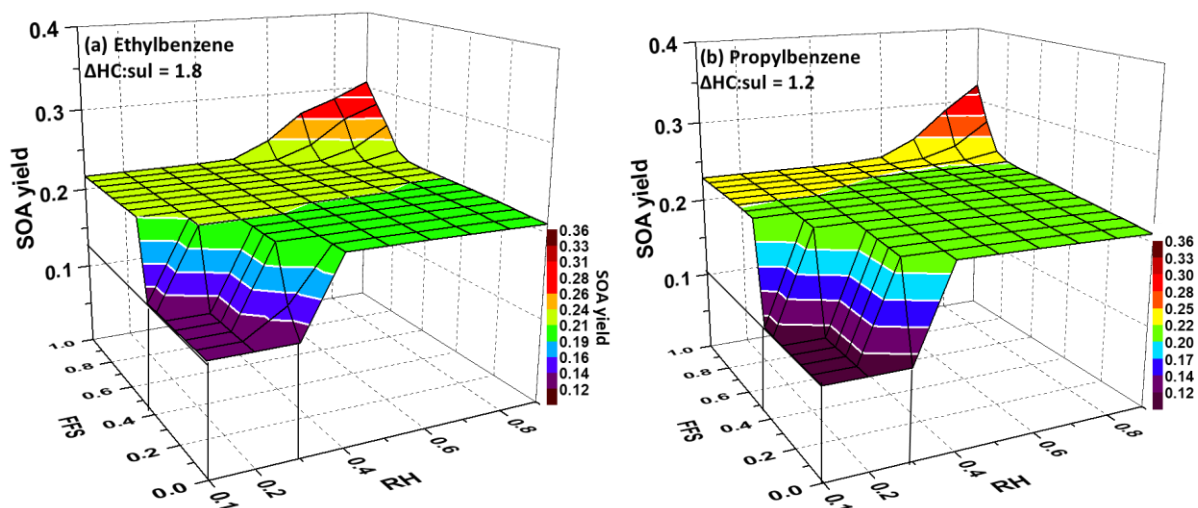


Figure S4: Simulated (a) ethylbenzene and (b) n-propylbenzene SOA yields ($Y_{\text{SOA}} = \Delta\text{OM}/\Delta\text{HC}$) as a function of relative humidity (RH: 0.1 ~ 0.9) and fractional free sulfate (FFS: 0 ~ 1), where $\text{FFS} = ([\text{SO}_4^{2-}] - 0.5[\text{NH}_4^+]) / [\text{SO}_4^{2-}]$ and is used to estimate aerosol acidity ($[\text{H}^+]$) in inorganic thermodynamic model. The RH and FFS are fixed during the simulations. The gas-phase simulations are based on the experimental condition of 06/14/2018 (Exp. Tol9 in Table 1) (initial HC concentration = 20 ppb, $\text{HC}/\text{NO}_x = 2$, sulfate mass concentration = 20 $\mu\text{g}/\text{m}^3$, and the mass ratio of the consumed HC to sulfate ($\Delta\text{HC:sulf}$) for ethylbenzene and propylbenzene = 1.8 and 1.2).

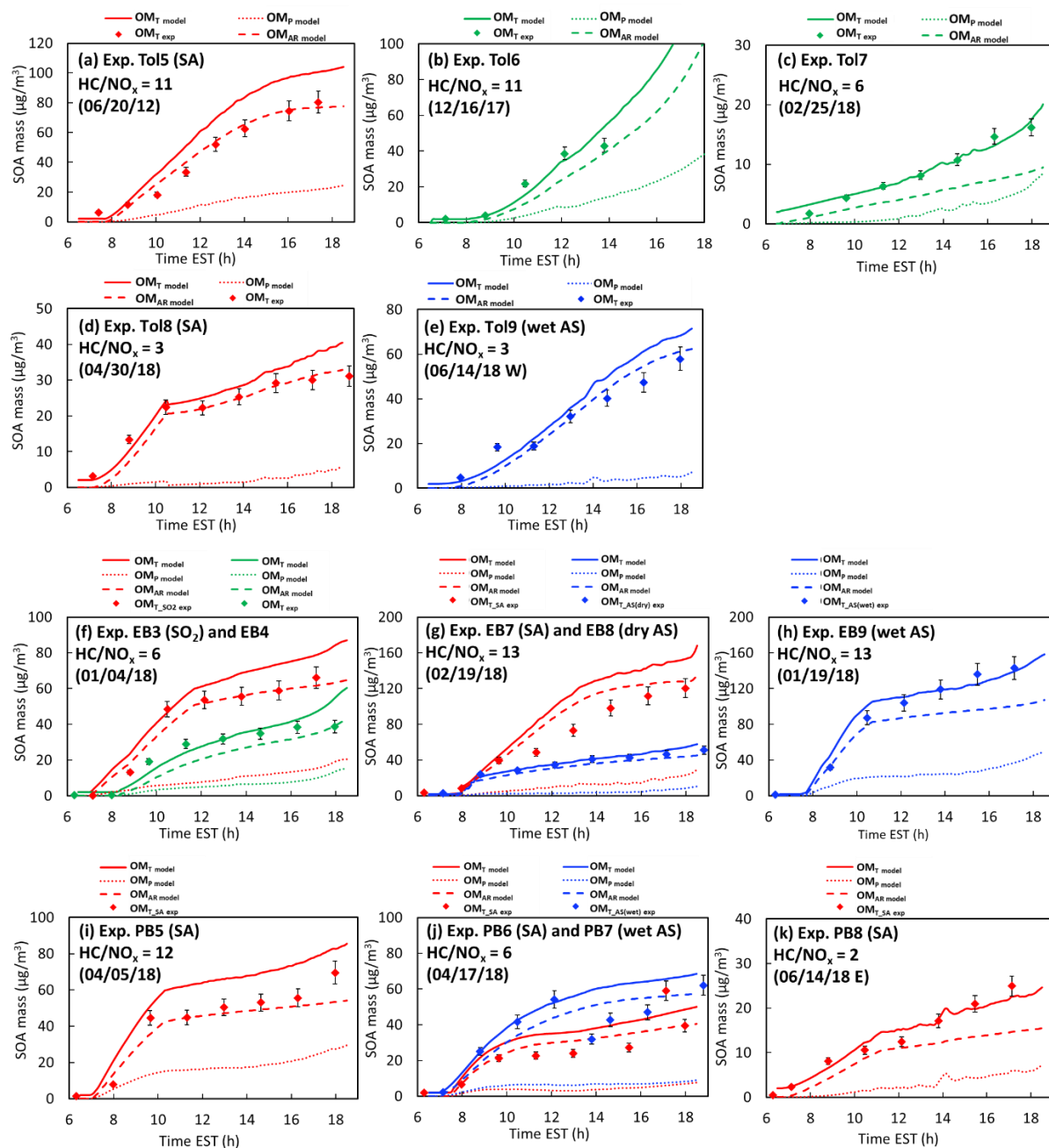


Figure S5: Time profiles of measured and modeled SOA mass concentrations for toluene (Tol: a-e), ethylbenzene (EB: f-h), and n-propylbenzene (PB: i-k) SOA under various NO_x levels in the presence/absence of inorganic seeded aerosol. The red, green, and blue colors indicate experiments with sulfuric acid seed, without inorganic seed, and with ammonium sulfate seed, respectively. SA denotes the direct-SA injection experiment. “wet” or “dry” in the figure denotes the physical state of the inorganic seed. Solid, dashed, and dotted lines denote total OM (OM_T), the OM from partitioning only (OM_P), and the OM from the aerosol-phase reactions (OM_{AR}), respectively. The uncertainty associated with experimentally measured OM

is 9 %, which is estimated from the uncertainties of measured OC and correction of particle wall loss. The experimental conditions are available in Table 1 in the manuscript.

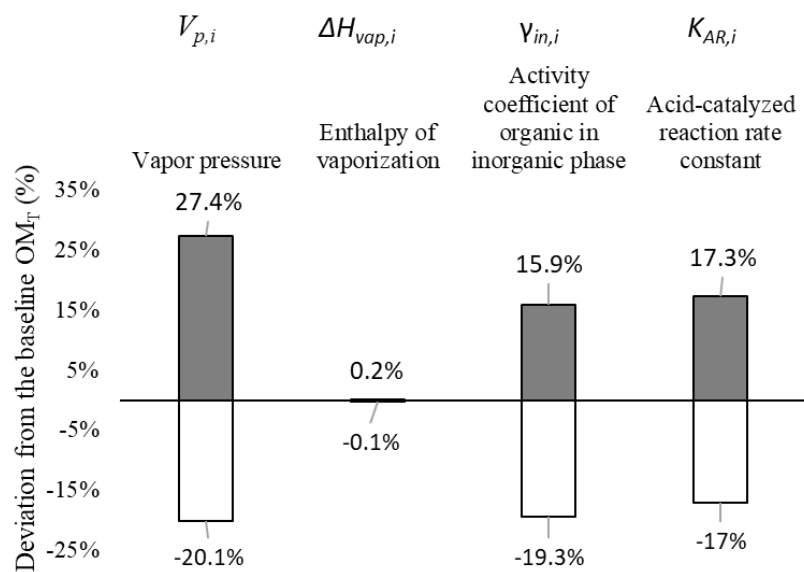


Fig. S6: Prediction of model uncertainty (simulated SOA mass deviated from the baseline SOA mass) due to the variation of major model parameters. The simulations employ the experiment performed on 06/14/2018 (Exp. Tol9 in Table 1). The estimated errors associated with vapor pressure (V_p), enthalpy of vaporization (H_{vap}), activity coefficients of the organics in the inorganic phase ($\gamma_{in,i}$) and oligomerization reaction rate constants in the inorganic phase ($k_{AC,i}$) were predicted with increasing/decreasing the V_p , H_{vap} , $\gamma_{in,i}$, and $k_{AC,i}$ by factors of 1.5, 1.1, 1.5, and 2, respectively.

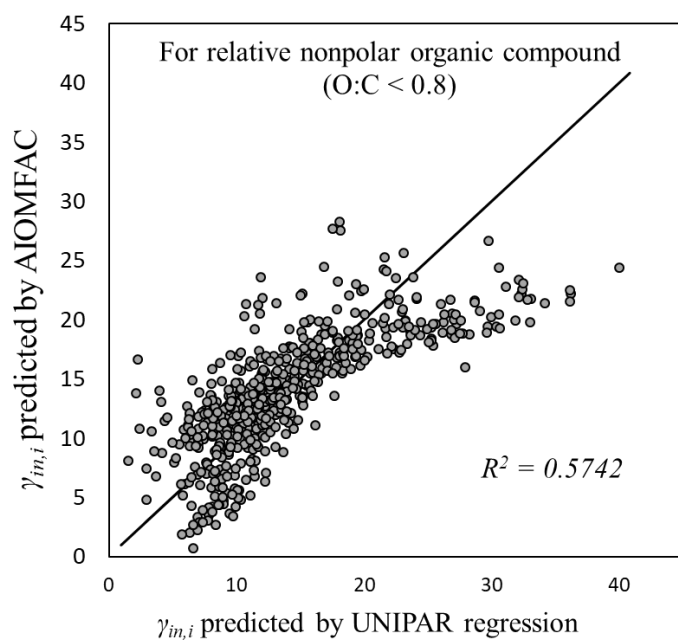


Figure S7: The $\gamma_{in,i}$ predicted by AIOMFAC were plotted against the $\gamma_{in,i}$ predicted by the regressions in Eq. 4 in the manuscript along with the line of $y = x$. R^2 is shown in the figure.

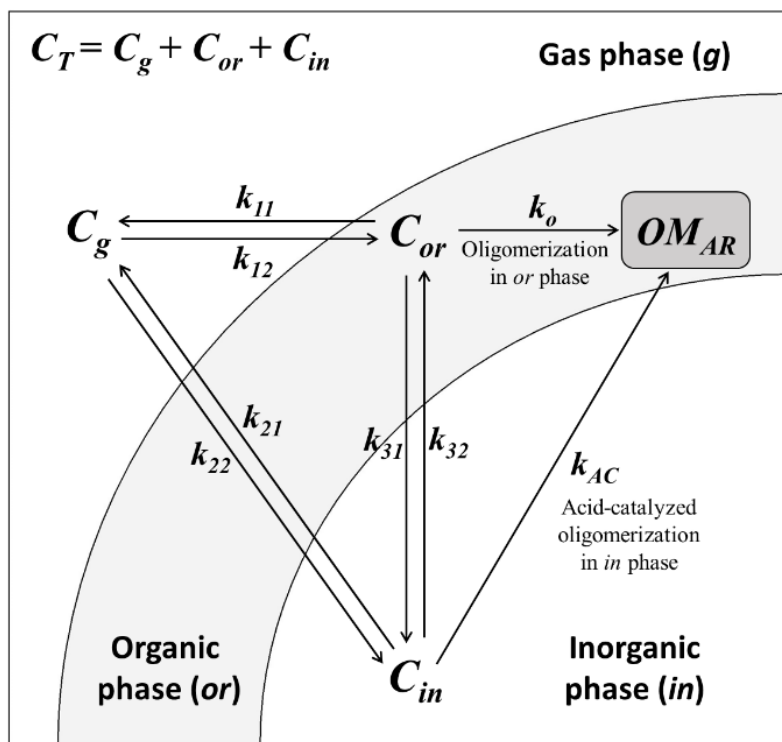


Figure S8. Simplified kinetic scheme for Fig. 1 in the manuscript for the products partitioning and aerosol-phase oligomerization in the UNIPAR model.